Journal of Zhejiang University SCIENCE A
ISSN 1673-565X (Print); ISSN 1862-1775 (Online)
www.zju.edu.cn/jzus; www.springerlink.com
E-mail: jzus@zju.edu.cn

Control strategy of hybrid fuel cell/battery distributed generation system for grid-connected operation

Masoud Aliakbar GOLKAR, Amin HAJIZADEH
(*Department of Electrical Engineering, K. N. Toosi University of Technology, Tehran, Iran*)
E-mail: golkar@eetd.kntu.ac.ir; aminhajizadeh@ee.kntu.ac.ir
Received Mar. 4, 2008; Revision accepted Jan. 15, 2009; Crosschecked Dec. 26, 2008

Abstract: This paper presents a control strategy of a hybrid fuel cell/battery distributed generation (HDG) system in distribution systems. The overall structure of the HDG system is given, dynamic models for the solid oxide fuel cell (SOFC) power plant, battery bank and its power electronic interfacing are briefly described, and controller design methodologies for the power conditioning units and fuel cell to control the power flow from the hybrid power plant to the utility grid are presented. To distribute the power between the fuel cell power plant and the battery energy storage, a neuro-fuzzy controller has been developed. Also, for controlling the active and reactive power independently in distribution systems, the current control strategy based on two fuzzy logic controllers has been presented. A Matlab/Simulink simulation model is developed for the HDG system by combining the individual component models and their controllers. Simulation results show the overall system performance including load-following and power management of the HDG system.

Key words: Battery, Fuel cell, Hybrid distributed generation, Intelligent control, Power control
doi:10.1631/jzus.A0820151 **Document code:** A **CLC number:** TP274; TM911.4

INTRODUCTION

Distributed generation systems based on the fuel cells (FCs) are expected to be important power sources in the future due to their many advantages, such as high efficiency, zero or low emission, and flexible modular structure (Hatziadoniu *et al*., 2002; Sedghisigarchi and Feliachi, 2002). However, due to their inherent characteristics these systems have disadvantages such as a long start-up time and poor response to instantaneous power demands. Hybrid fuel cell/battery distributed generation (HDG) systems are introduced to make the best use of the advantages of each individual device (Yalcinoz and Alam, 2008). HDG systems can be placed at any site in a power distribution system for grid reinforcement and active and reactive power control. Recently, some researches have concentrated on control of hybrid power sources. In (Gao *et al*., 2004; Jiang *et al*., 2005; 2007) the control strategies for a hybrid fuel cell/battery system have been presented. A detailed dynamic model, design, and simulation of a wind/fuel cell/ultra-capacitor-based hybrid power generation system has been developed using a novel topology to complement each other and to alleviate the effects of wind speed variations (Onar *et al*., 2006). In (Uzunoglu and Alam, 2006), the dynamic modeling of a combined proton exchange membrane fuel cell (PEMFC) and ultra capacitor bank system, as well as the developing of power flow control strategies have been considered. In (Hajizadeh and Golkar, 2007b), a fuzzy logic algorithm has been used to determine the FC output power based on the external power requirement, the battery state of charge (SOC) and FC temperature. But Hajizadeh and Golkar (2007b) presented only the active power sharing in the hybrid system, and did not consider the reactive power control. Up to now a study on the control structure of the HDG system has not been considered completely. Also, the power must be distributed between generation sources optimally. Hence, this paper presents modeling and a power control strategy of an HDG

system with real and reactive power control capability. The dynamic model of each component is investigated. Then the control structure based on the developed model is presented.

MODELING OF HYBRID DISTRIBUTED GENERATION SYSTEM

To meet the system operational requirements, an HDG system needs to be interfaced through a set of power electronic devices (Hajizadeh and Golkar, 2007a). The interface is very important as it affects the operation of the hybrid fuel cell/battery system as well as the power grid. Fig.1 shows the schematic diagram of the HDG system proposed in this study. This section describes the dynamic models for the main components of the system shown in Fig.1, namely for the solid oxide fuel cell (SOFC) power plant, the battery, the DC/DC converters, and the three-phase inverter.

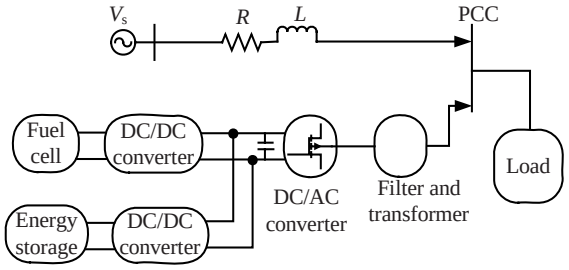

Fig.1 Block diagram of a hybrid fuel cell/battery distributed generation system

Solid oxide fuel cell model

The model of an SOFC power plant used in this study is based on the dynamic SOFC stack model developed and validated in (Padulles *et al*., 2000). The FC model used in this study is realized in Matlab and Simulink. The following equation models the voltage of the FC stack:

$$V_{\mathrm{fc}} = N_0\left(E_0 + \frac{RT}{2F}\ln\left(\frac{(P_{\mathrm{H}_2}P_{\mathrm{O}_2})^{0.5}}{P_{\mathrm{H}_2\mathrm{O}}}\right)\right) - rI_{\mathrm{f0}}, \quad (1)$$

with P_{H_2}, $P_{\mathrm{H}_2\mathrm{O}}$, P_{O_2} determined by the following differential equations:

$$\begin{cases} \dot{P}_{\mathrm{H}_2} = -\dfrac{1}{t_{\mathrm{H}_2}}\left(P_{\mathrm{H}_2} + \dfrac{1}{K_{\mathrm{H}_2}}(q_{\mathrm{H}_2}^{\mathrm{in}} - 2K_{\mathrm{r}}I_{\mathrm{fc}})\right), \\ \dot{P}_{\mathrm{H}_2\mathrm{O}} = -\dfrac{1}{t_{\mathrm{H}_2\mathrm{O}}}\left(P_{\mathrm{H}_2\mathrm{O}} + \dfrac{2}{K_{\mathrm{H}_2\mathrm{O}}}K_{\mathrm{r}}I_{\mathrm{fc}}\right), \\ \dot{P}_{\mathrm{O}_2} = -\dfrac{1}{t_{\mathrm{O}_2}}\left(P_{\mathrm{O}_2} + \dfrac{1}{K_{\mathrm{O}_2}}(q_{\mathrm{O}_2}^{\mathrm{in}} - K_{\mathrm{r}}I_{\mathrm{fc}})\right), \end{cases} \quad (2)$$

where N_0 is the number of series FCs in the stack; E_0 is the standard no-load voltage (V); R is the universal gas constant (×101.325 kPa/(kmol·K)); T is the absolute temperature (K); I_{f0} is the current of the FC stack (A); F is Faraday's constant (C/kmol); K_{H_2}, $K_{\mathrm{H}_2\mathrm{O}}$ and K_{O_2} are the molar constants (kmol/(101.325 kPa·s)) of the hydrogen, water, and oxygen valves, respectively; K_{r} is the modeling constant (kmol/(s·A)); P_{H_2}, $P_{\mathrm{H}_2\mathrm{O}}$ and P_{O_2} are the partial pressure (×101.325 kPa) of hydrogen, water and oxygen, respectively; $q_{\mathrm{H}_2}^{\mathrm{in}}$ is the hydrogen input flow (kmol/s); $q_{\mathrm{O}_2}^{\mathrm{in}}$ is the oxygen input flow (kmol/s); r is the FC internal resistance (Ω); t_{H_2}, t_{O_2} and $t_{\mathrm{H}_2\mathrm{O}}$ are the hydrogen, oxygen and water time constants (s), respectively.

The K_{r} constant is defined by the relationship between the rate of reactant hydrogen and the FC current:

$$q_{\mathrm{H}_2}^{\mathrm{r}} = \frac{N_0 I}{2F} = 2K_{\mathrm{r}}I, \quad (3)$$

where $q_{\mathrm{H}_2}^{\mathrm{r}}$ is the hydrogen flow that reacts (kmol/s).

Another important operating variable is the reactant utilization, U_{f}, referred to as the fraction of the total fuel (or oxidant) introduced into an FC that reacts electrochemically:

$$U_{\mathrm{f}} = \frac{q_{\mathrm{H}_2}^{\mathrm{in}} - q_{\mathrm{H}_2}^{\mathrm{out}}}{q_{\mathrm{H}_2}^{\mathrm{in}}} = \frac{q_{\mathrm{H}_2}^{\mathrm{r}}}{q_{\mathrm{H}_2}^{\mathrm{in}}}, \quad (4)$$

where $q_{\mathrm{H}_2}^{\mathrm{out}}$ is the hydrogen output flow (kmol/s).

A high utilization is considered desirable because it minimizes the required fuel and oxidant flow, for a minimum fuel cost and compressor load and size.

Battery model

The battery model used is essentially two RC circuits connected in series, as shown in Fig.2.

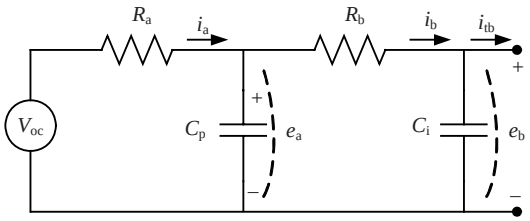

Fig.2 RC model of the battery

The internal resistance (R_a) and the open circuit voltage (V_{oc}) are functions of the battery state of charge (Q_{SOC}). The voltages across the two capacitors and Q_{SOC} are the three state variables for the battery (Hajizadeh and Golkar, 2007b):

$$V_{oc} = 338.8(0.942\,46 + 0.057\,54Q_{SOC}), \tag{5}$$

$$R_a C_p \frac{de_a}{dt} + \frac{R_a + R_b}{R_b} e_a = V_{oc} + \frac{R_a}{R_b} e_b, \tag{6}$$

$$R_b C_i \frac{de_b}{dt} + e_b = e_a - R_b i_{tb}, \tag{7}$$

where R_a is the battery internal resistance (Ω); R_b is the terminal ohmic resistance (Ω); C_i is the incipient capacitance (F); C_p is the polarization capacitance (F); V_{oc} is the charge-dependent open circuit voltage (V).

The battery state of charge, Q_{SOC}, is the only state variable of the battery system,

$$\frac{dQ_{SOC}}{dt} = \frac{I_{tb}}{Q_m}, \tag{8}$$

where Q_m is the maximum battery charge (A·h), and I_{tb} is the battery current (A), calculated by

$$I_{tb} = \frac{V_{oc} - \sqrt{V_{oc}^2 - 4(R_a + R_b)P_b}}{2(R_a + R_b)}, \tag{9}$$

where P_b is the output power (W) of the battery.

DC/DC converter modeling

To connect an FC to an external power system, it is necessary to boost the FC voltage or to increase the number of cells. The role of the DC/DC boost converter is to increase the FC voltage, to control the FC power, and to regulate the voltage. Fig.3 shows the DC/DC converter model. This boost converter is described by the following two nonlinear state space averaged equations (Hajizadeh and Golkar, 2007a):

$$\begin{cases} \dfrac{dX_1}{dt} = \dfrac{1-d}{L} X_2 + \dfrac{d}{L} U, \\ \dfrac{dX_2}{dt} = \dfrac{-(1-d)}{C} X_1 - \dfrac{X_2}{RC}, \end{cases} \tag{10}$$

where d is the duty cycle of the switching device; U is the input voltage (V); X_1 is the inductor current (A); X_2 is the capacitor voltage (V).

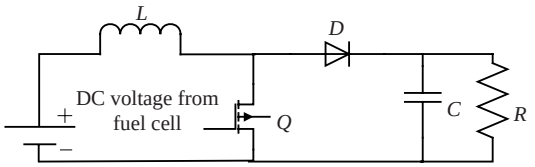

Fig.3 DC/DC converter model

DC/AC converter modeling

Various power electronic circuits have been proposed to interface different energy sources with the AC loads and utility grid. Pulse-width-modulated (PWM) voltage source inverters (VSIs) are widely used to interconnect an FC energy system to the AC loads and utility grid. For this purpose, a dynamic model of the voltage source inverter has been developed, as given in Fig.4. To reduce the harmonics, filters are connected between the converter and the grid, represented by L_s and R_s, respectively. In Fig.4, V_{ia}, V_{ib}, V_{ic} are the three-phase AC voltage outputs of the inverter, and i_a, i_b, i_c are the three-phase AC current outputs of the inverter. The bus voltages of the grid are V_{sa}, V_{sb}, V_{sc}.

The dynamic model of the three-phase VSC is represented in (Yang *et al*., 2001; Hajizadeh and Golkar, 2007a) as

$$\frac{di_k}{dt} = -\frac{R_s}{L_s} i_k + \frac{1}{L_s}(V_{ik} - V_{sk}), \tag{11}$$

where k=a, b, or c; L_s is the inductance of the line connecting to the load (H); R_s is the resistance of the line connecting to the load (Ω).

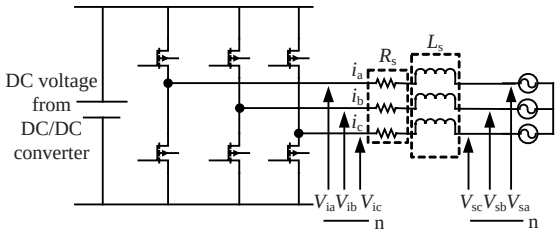

Fig.4 DC/AC converter model

To develop the dynamic model, the states Eq.(11) are transformed to the system synchronous reference frame as

$$\begin{cases}\dfrac{\mathrm{d}i_q}{\mathrm{d}t}=\dfrac{-R_s\omega_s}{L_s}i_q-\omega_s i_d+\dfrac{\omega_s}{L_s}mV_{dc}\sin(\delta+\theta_s)-\dfrac{\omega_s}{L_s}V_s\sin\theta_s,\\ \dfrac{\mathrm{d}i_d}{\mathrm{d}t}=\dfrac{-R_s\omega_s}{L_s}i_d+\omega_s i_q+\dfrac{\omega_s}{L_s}mV_{dc}\cos(\delta+\theta_s)-\dfrac{\omega_s}{L_s}V_s\cos\theta_s,\end{cases} \tag{12}$$

where V_{dc} is the DC bus terminal voltage (V); V_s is the load terminal voltage (V); δ is the phase angle of the AC voltage (rad); m is the inverter modulation index; ω_s is the angular frequency and $\theta_s=\omega_s t$.

CONTROL STRATEGY OF THE HDG SYSTEM

In this section, the control strategy of the HDG system has been presented. The overall control structure has been illustrated in Fig.5, which includes the power flow controller and local controllers for power conditioning units and the FC. The term 'power flow control' refers to the design of the higher-level control algorithm that determines the proper power level to be generated, and its split between the two power sources. The details for this control structure are explained below.

Power flow control between power sources

The power flow control strategy is designed to determine the proper power level between the FC stack and battery energy storage, while satisfying the power demand from the load and maintaining adequate energy in the energy storage device. Frequent power demand variations and unpredictable load profile are unavoidable uncertainties. Also, nonlinear and often time-varying subsystems add to the complexity of the structure of a hybrid system.

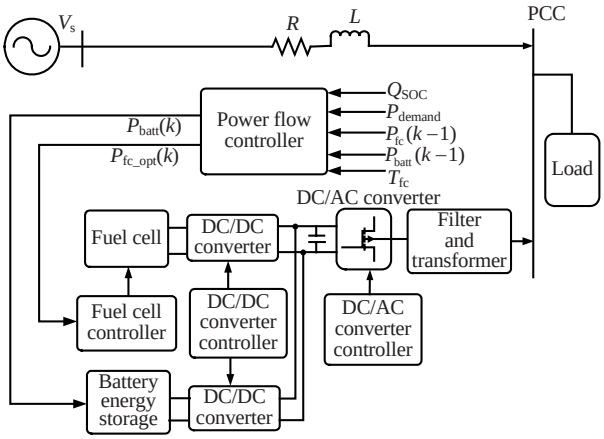

Fig.5 Control strategy structure for a hybrid distributed generation system

Moreover, the control strategy must act online to distribute the power between power sources based on the system conditions. Hence an online control strategy based on fuzzy logic has been proposed for instantaneous power management in (Hajizadeh and Golkar, 2007b). But the parameters of the proposed fuzzy controller during the power management have been considered constantly and it has not the adaptive property. To improve the performance of the power flow control strategy, we present the neuro-fuzzy control strategy in this study. The term 'neuro-fuzzy system' refers to combinations of neural networks and fuzzy systems. In the proposed control structure, the FC power is determined optimally according to the demand power (P_{demand}), the battery power (P_{batt}), the battery's state of charge (Q_{SOC}) and the FC power in one step before ($P_{fc}(k-1)$). In addition to generating the FC power optimally, the efficiency maps of the FC power source and battery energy storage are used (Figs.6 and 7). As shown in Fig.6, the maximum efficiency of FC is around the power of 30 kW; according to Fig.7, the maximum efficiency of battery energy storage during the charge and discharge cycles is around the state of charge of 75%. Moreover, in order to operate the FC stack at an optimal fuel utilization point (approximately 85%) (Zhu and Tomsovic, 2002), the FC controller is to maintain an optimal hydrogen utilization, $U_{f,opt}$, around 85%. So, the error function in Eq.(13) has been used for the neuro-fuzzy control strategy to train the parameters of membership functions in fuzzy controllers. This process shall be explained in the next subsection in detail.

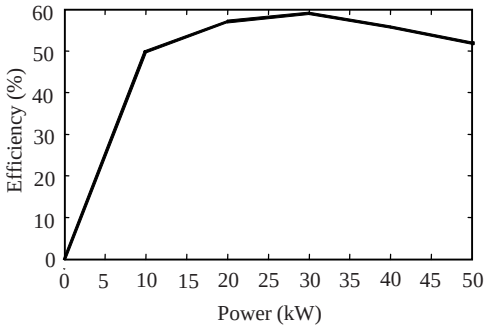

Fig.6 Efficiency map of the fuel cell stack

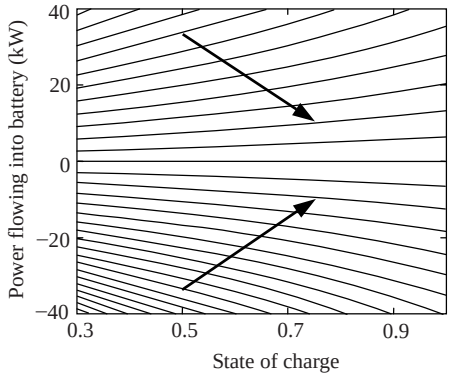

Fig.7 Charge and discharge diagram of battery

$$E(k)=\sum_{k=1}^{N-1}\Big(w_1(P_{\mathrm{fc}}(k)-P_{\mathrm{fc\_opt}})^2+w_2(Q_{\mathrm{SOC}}(k)-Q_{\mathrm{SOC\ opt}})^2 +w_3(U_{\mathrm{f}}(k)-U_{\mathrm{f\_opt}})^2\Big), \tag{13}$$

where N is the duration of the power demand; w_1, w_2 and w_3 are the weighting coefficients representing the relative importance of the objectives and they must satisfy

$$w_1+w_2+w_3=1. \tag{14}$$

Neuro-fuzzy control strategy

Recently, the combination of neural networks and fuzzy logic has received attention. Neural networks bring into this union the ability to learn, but also require an excessive number of iterations for training of complex systems. Fuzzy logic offers a system model based on membership functions and a rule base, but requires an explicit stating of the IF/THEN rules. In this type of model, the condition part uses linguistic variables and the conclusion part is represented by a numerical value that is considered as a function of the system condition expressed with the variables x_1, x_2, …, x_m:

$$\omega^l=g(x_1,x_2,...,x_m). \tag{15}$$

The neuro-fuzzy algorithm uses membership functions of Gaussian type. With Gaussian fuzzy sets, the algorithm is capable of utilizing all information contained in the training set to calculate each rule conclusion, which is different when using triangular partitions. Fig.8 illustrates the neuro-fuzzy scheme for an example with two input variables (x_1, x_2) and one output variable (y). In the first stage of the neuro-fuzzy scheme, the two inputs are codified into linguistic values by the set of Gaussian membership functions (MFs) attributed to each variable. The second stage calculates each rule $R^{(l)}$ as its respective activation degree. Last, the inference mechanism weights each rule conclusion $\omega^{(l)}$, initialized by the cluster-based algorithm, using the activation degree computed in the second stage. The error signal between the model inferred value Y and the respective measured value (or teaching value) y', is used by the gradient descent method to adjust each rule conclusion. The algorithm modifies the values of $\omega^{(l)}$ to minimize an objective function E usually expressed by the mean quadratic error:

$$E=\frac{1}{2}[Y(\boldsymbol{x}'(k))-y'(k)]^2. \tag{16}$$

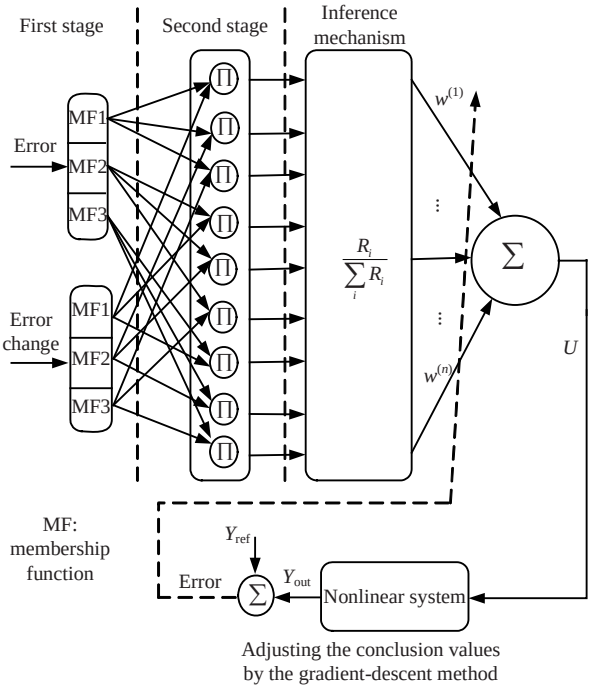

Fig.8 The neuro-fuzzy control structure

In Eq.(16), the value $y'(k)$ is the desired output value related with the condition vector $\boldsymbol{x}'(k) = [x'_1, x'_2, \ldots, x'_m]$. The element $Y(\boldsymbol{x}'(k))$ is the inferred response to the same condition vector $\boldsymbol{x}'(k)$ and computed by

$$Y(\boldsymbol{x}'(k)) = \frac{\sum_{l=1}^{c}\left(\prod_{j=1}^{m}\mu_{A_{j=1}^{(l)}}(x'_j(k))\right)\omega^{(l)}(k)}{\sum_{l=1}^{c}\left(\prod_{j=1}^{m}\mu_{A_{j=1}^{(l)}}(x'_j(k))\right)}, \quad (17)$$

where $\mu_{A_{j=1}^{(l)}}$ represent the Gaussian membership functions.

Eq.(17) establishes adjustment of each conclusion $\omega^{(l)}$ by the gradient-descent method. The symbol α is the learning rate parameter, and t indicates the number of learning iterations executed by

$$\omega^{(l)}(t+1) = \omega^{(l)}(t) - \alpha\frac{\partial E}{\partial \omega^{(l)}}. \quad (18)$$

The inference function Eq.(17) depends on $\omega^{(l)}$ only through its numerator. The expression composing the numerator is now denoted by a and is shown as

$$a = \sum_{l=1}^{c}\left(\prod_{j=1}^{m}\mu_{A_{j=1}^{(l)}}x'_j(k)\right)\omega^{(l)}(k). \quad (19)$$

The denominator of function Eq.(17) is dependent on a term $d^{(l)}$, defined in Eq.(20), and denoted by b in Eq.(21).

$$d^{(l)} = \prod_{j=1}^{m}\mu_{A_{j=1}^{(l)}}x'_j(k), \quad (20)$$

$$b = \sum_{l=1}^{c}d^{(l)}. \quad (21)$$

To calculate the adjustment of each conclusion value $\omega^{(l)}$, it is necessary to compute the variation of the objective function E, ∂E, in relation to the variation that occurs in $\omega^{(l)}$ in the anterior instant, $\partial\omega^{(l)}$. Therefore, using the chain rule to calculate $\frac{\partial E}{\partial \omega^{(l)}}$ results in

$$\frac{\partial E}{\partial \omega^{(l)}} = \frac{\partial E}{\partial Y}\frac{\partial Y}{\partial a}\frac{\partial a}{\partial \omega^{(l)}}. \quad (22)$$

The use of the chain rule looks for the term contained in E that is directly dependent on the value to be adjusted, i.e., the conclusion value $\omega^{(l)}$. Therefore, we can verify by chain Eq.(22) that: it starts with E dependent on the Y value, the Y value depends on term α and, at last, the expression a is a function of $\omega^{(l)}$. After some computation, the adjustment to be made in $\omega^{(l)}$ can be interpreted as being proportional to the error between the neuro-fuzzy model response and the supervising value, but weighted by the contribution of rule (l), denoted by $d^{(l)}$, to the final neuro-fuzzy inference:

$$\omega^{(l)}(t+1) = \omega^{(l)}(t) - \alpha[Y(\boldsymbol{x}'(k)) - y'(k)]d^{(l)}\Big/\sum_{l=1}^{c}d^{(l)}. \quad (23)$$

Controller designs for power electronic devices and fuel cell

The final part of the control structure is the designing of the local controllers for the FC power plant, DC/DC converter and grid-connected inverter to track the proposed set points. Each component will be controlled by its own local controller so that the subsystem is stable and the power demand is satisfied as much as possible. The details of these local controllers have been described completely in (Hajizadeh and Golkar, 2007b) and only the control diagram of each component has been shown here. Fig.9a illustrates the control structure of the FC system. According to the error between the reference current and actual current, the output of the fuzzy logic controller is the hydrogen molar flow $q_{H_2\_ref}$. Moreover, the control structures of the DC/DC converter and grid-connected inverter have been presented in Figs.9b and 9c, respectively. In the DC/DC converter controller, the error between the output voltage and reference voltage of the DC/DC converter is used as input to the fuzzy logic controller. The control signal is fed to the PWM generator. The boost converter generates output voltage based upon the duty ratio provided by the PWM generator. Also, to control the real and reactive power in the grid-connected inverter independently, two fuzzy logic controllers have been used. To achieve the active and the reactive power control tasks, the currents i_{q_ref} and i_{d_ref} are assigned to the output of the fuzzy logic controllers. The inputs of these controllers are the errors between the reference and actual values of the active and the reactive powers that applied respectively.

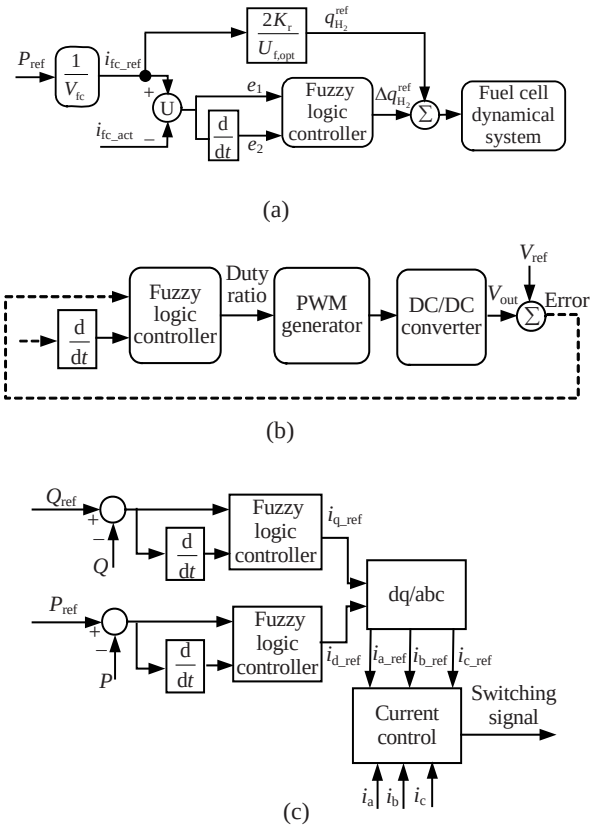

Fig.9 Fuzzy logic controller for the fuel cell (a), DC/DC converter (b), and DC/AC converter (c)

SIMULATION AND DISCUSSION

A simulation model of the HDG system, as explained in Section 2, was built in Matlab/Simulink to validate the effectiveness of the proposed control strategy. The SOFC system operates in parallel with a battery bank connected to the DC bus via two DC/DC converters. The battery bank serves as a short-duration power source to meet the load demand that cannot be met by the FC system, particularly during transient- or peak-demand periods. The system was tested under operating conditions to investigate its power management between power sources and to deliver active and reactive powers to the grid. The SOFC system parameters in this study are given in Table 1. The power conditioning unit parameters (including DC/DC and DC/AC converters) and battery system specifications (Hajizadeh and Golkar, 2007a; 2007b) are given in Tables 2 and 3, respectively.

Table 1 Fuel cell system model parameters

Parameter	Value
Faraday's constant, F (C/kmol)	96 484 600
Hydrogen time constant, t_{H_2} (s)	26.1
Hydrogen valve molar constant, K_{H_2}	8.43×10^{-4}
K_r constant (=N_0/(4F))	9.9497×10^{-7}
No-load voltage, E_0 (V)	0.6
Number of cells, N_0	384
Oxygen time constant, t_{O_2} (s)	2.91
Oxygen valve molar constant, K_{O_2}	2.52×10^{-3}
Fuel cell internal resistance, r (Ω)	0.126
Fuel cell absolute temperature, T (K)	343
Universal gas constant, R (J/(kmol·K))	8314.47
Utilization factor, U_f	0.8
Water time constant, t_{H_2O} (s)	78.3
Water valve molar constant, K_{H_2O}	2.81×10^{-4}

Table 2 Power conditioning units parameters

DC/AC converter parameter	Value
Rated voltage	540 V/220 V
Rated power (kW)	100
Resistance, R_s (mΩ)	0.9
Inductor, L_s (mH)	0.01
Frequency, f_s (Hz)	50
DC/DC converter parameter	**Value**
Rated voltage	200 V/540 V
Resistance, R (Ω)	2.3
Capacitance, C (mF)	1.5
Inductor, L (μH)	415

Table 3 Battery model parameters

Parameter	Value
Capacity, Q_m (A·h)	50
Number of modules	25
Rated voltage (V)	308
Internal resistance, R_a (Ω)	0.015×(100±25)%
Terminal resistance, R_b (Ω)	0.015×(100±25)%
Incipient capacitance, C_i (F)	3
Polarization capacitance, C_p (F)	3
Minimum state of charge (%)	65
Maximum state of charge (%)	80

The profile of active power demand (Fig.10) has a significant effect on determining the power management strategy. It is a good representation of transient states and it has a periodic property. Also, the reference value of reactive power was set as 35 kV·A for this case study. The output power of the FC system was limited to 50 kW, and the battery bank system can

sustain an extra load of 25 kW for 100 s during peak demand periods. The inverter was assumed to have an input of 200 V DC and an output of 220 V AC. In the DC/AC inverter, fuzzy controllers were used to control the reactive power and active power to adjust the modulation index and phase angle according to the load power variations. Simulation results were obtained for the time interval between 0 and 250 s. Fig.11a shows the FC power that changes around the power of 30 kW. In this case, as shown in Fig.6, the maximum efficiency of the FC system is satisfied. The battery power is shown in Fig.11b. As illustrated, the battery power is negative when the FC power is bigger than the load power. While the power demand is increasing, the FC power is raised smoothly, and the rest of the load power is provided by battery. From Figs.11a and 11b, it is evident that the FC system and battery bank share this load requirement.

Fig.12a shows the variation of the battery bank current between negative (charging) and positive (discharging) values according to the required load demand. Moreover, the battery bank voltage is affected by the load conditions, as seen in Fig.12b. If the power produced by the FC is more than the required power of the load, the extra power of the FC is used to charge the battery, and the battery SOC goes high. The results show that the SOC can be maintained at a reasonable level, as seen in Fig.12c.

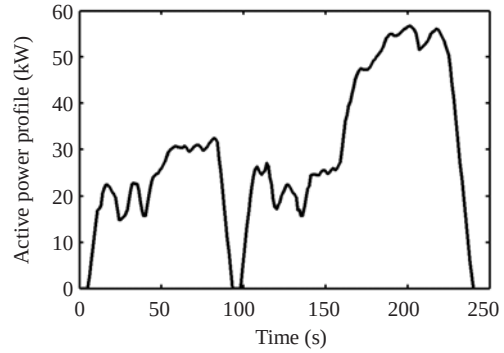

Fig.10 The profile of active power

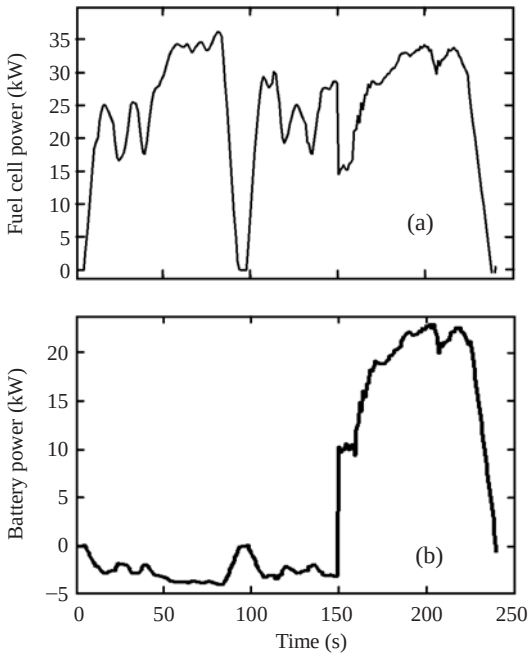

Fig.11 Variation of fuel cell system output power (a) and battery bank output power (b)

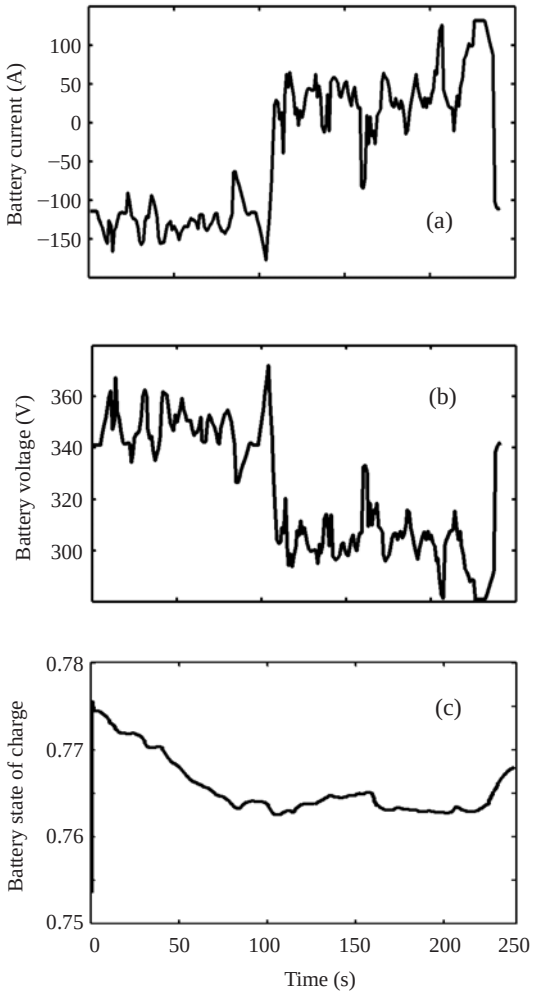

Fig.12 (a) Variation of battery bank charging and discharging current according to the load profile; (b) Variation of battery bank output voltage; (c) Variation of battery bank state of charge

Fig.13 illustrates the utilization factor of the FC, which varies around 0.85 during the operation of the FC. From Fig.13, it can be observed that the FC operation has been regulated at the optimal operating point. Fig.14 reflects the reactive power response of the HDG system, which matches the reference value sets for the reactive power.

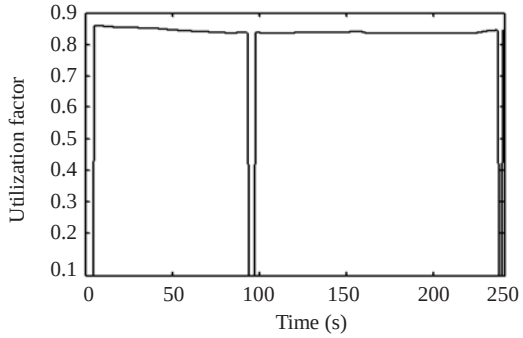

Fig.13 Variation of fuel cell utilization factor

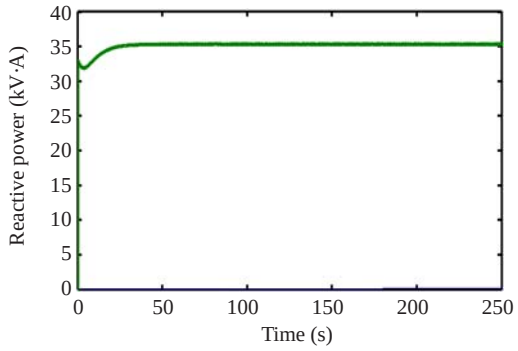

Fig.14 Variation of the reactive power delivered to the grid

CONCLUSION

This paper presents an adaptive neuro-fuzzy control strategy to manage the active power between the two power sources—fuel cell and battery—in a hybrid fuel cell/battery distributed generation system. A validated SOFC dynamic model is used to model the FC power plant. The dynamic models for the battery bank, the boost DC/DC converter and the three-phase grid-connected inverter are also discussed. Simulation results of the case studies show that the real and reactive power delivered from the FC system to the utility grid can be controlled as desired, while the battery's state of charge and utilization factor of FC are maintained well within the prescribed range.

References

Gao, L., Jiang, Z., Dougal, R.A., 2004. An actively controlled fuel cell/battery hybrid to meet pulsed power demands. *J. Power Sources*, **130**(1-2):202-207. [doi:10.1016/j.jpowsour.2003.12.052]

Hajizadeh, A., Golkar, M.A., 2007a. Intelligent Control of Fuel Cell Distributed Generation Systems. 14th Int. Conf. on Intelligent System Applications to Power Systems, p.1-7. [doi:10.1109/ISAP.2007.4441591]

Hajizadeh, A., Golkar, M.A., 2007b. Intelligent power management strategy of hybrid distributed generation system. *Int. J. Electr. Power Energy Syst.*, **29**(10):783-795. [doi:10.1016/j.ijepes.2007.06.025]

Hatziadoniu, C.J., Lobo, A.A., Pourboghrat, F., Daneshdoost, M., 2002. A simplified dynamic model of grid-connected fuel-cell generators. *IEEE Trans. Power Del.*, **17**(2):467-473. [doi:10.1109/61.997919]

Jiang, Z., Gao, L., Dougal, R.A., 2005. Flexible multiobjective control of power converter in active hybrid fuel cell/battery power sources. *IEEE Trans. Power Electr.*, **20**(1):244-253. [doi:10.1109/TPEL.2004.839782]

Jiang, Z., Gao, L., Dougal, R.A., 2007. Adaptive control strategy for active power sharing in hybrid fuel cell/battery power sources. *IEEE Trans. Energy Conv.*, **22**(2):507-515. [doi:10.1109/TEC.2005.853747]

Onar, O.C., Uzunoglu, M., Alam, M.S., 2006. Dynamic modeling, design and simulation of a wind/fuel cell/ultra-capacitor-based hybrid power generation system. *J. Power Sources*, **161**(1):707-722. [doi:10.1016/j.jpowsour.2006.03.055]

Padulles, J., Ault, G.W., McDonald, J.R., 2000. An integrated SOFC plant dynamic model for power systems simulation. *J. Power Sources*, **86**(1-2):495-500. [doi:10.1016/S0378-7753(99)00430-9]

Sedghisigarchi, K., Feliachi, A., 2002. Control of Grid-connected Fuel Cell Power Plant for Transient Stability Enhancement. Proc. IEEE Power Engineering Society Winter Power Meeting, p.383-388. [doi:10.1109/PESW.2002.985024]

Uzunoglu, M., Alam, M.S., 2006. Dynamic modeling, design, and simulation of a combined PEM fuel cell and ultra-capacitor system for stand-alone residential applications. *IEEE Trans. Energy Conv.*, **21**(3):767-775. [doi:10.1109/TEC.2006.875468]

Yalcinoz, T., Alam, M.S., 2008. Improved dynamic performance of hybrid PEM fuel cells and ultracapacitors for portable applications. *Int. J. Hydr. Energy*, **33**(7):1932-1940. [doi:10.1016/j.ijhydene.2008.01.027]

Yang, Z., Shen, C., Zhang, L., Crow, M.L., Atcitty, S., 2001. Integration of a StatCom and battery energy storage. *IEEE Trans. Power Syst.*, **16**(2):254-260. [doi:10.1109/59.918295]

Zhu, Y., Tomsovic, K., 2002. Development of models for analyzing the load-performance of microturbines and fuel cells. *Electr. Power Syst. Res.*, **62**(1):1-11. [doi:10.1016/S0378-7796(02)00033-0]